

# Iron $K\alpha$ emission in type-I and type-II Active Galactic Nuclei

C. Ricci<sup>1\*</sup>, Y. Ueda<sup>1</sup>, S. Paltani<sup>2</sup>, K. Ichikawa<sup>1</sup>, P. Gandhi<sup>3</sup>, and H. Awaki<sup>4</sup>

<sup>1</sup>Department of Astronomy, Kyoto University, Oiwake-cho, Sakyo-ku, Kyoto 606-8502

<sup>2</sup>Department of Astronomy, University of Geneva, ch. d'Ecogia 16, 1290 Versoix, Switzerland

<sup>3</sup>Department of Physics, University of Durham, South Road, Durham DH1 3LE, UK

<sup>4</sup>Department of Physics, Ehime University, Matsuyama, 790-8577, Japan

Received; accepted

## ABSTRACT

The narrow Fe  $K\alpha$  line is one of the main signatures of the reprocessing of X-ray radiation from the material surrounding supermassive black holes, and it has been found to be omnipresent in the X-ray spectra of active galactic nuclei (AGN). In this work we study the characteristics of the narrow Fe  $K\alpha$  line in different types of AGN. Using the results of a large *Suzaku* study we find that Seyfert 2s have on average lower Fe  $K\alpha$  luminosities than Seyfert 1s for the same 10–50 keV continuum luminosity. Simulating dummy Seyfert 1s and Seyfert 2s populations using physical torus models of X-ray reflected emission, we find that this difference can be explained by means of different average inclination angles with respect to the torus, as predicted by the unified model. Alternative explanations include differences in the intensities of Compton humps, in the photon index distributions or in the average iron abundances. We show that the ratio between the flux of the broad and narrow Fe  $K\alpha$  line in the 6.35–6.45 keV range depends on the torus geometry considered, and is on average < 25% and < 15% for type I and type II AGN, respectively. We find evidence of absorption of the narrow Fe  $K\alpha$  line flux in Compton-thick AGN, which suggests that part of the reflecting material is obscured. We estimate that on average in obscured AGN the reflected radiation from neutral material is seen through a column density which is 1/4 of that absorbing the primary X-ray emission. This should be taken into account in synthesis models of the CXB and when studying the luminosity function of heavily obscured AGN. We detect the first evidence of the X-ray Baldwin effect in Seyfert 2s, with the same slope as that found for Seyfert 1s, which suggests that the mechanism responsible for the decrease of the equivalent width with the continuum luminosity is the same in the two classes of objects.

**Key words:** Galaxies: Seyferts – X-rays: galaxies – Galaxies: active – Galaxies: nuclei

## 1 INTRODUCTION

Active Galactic Nuclei (AGN) emit a large fraction of their luminosity in the X-rays. Such an emission is believed to originate from Comptonisation of optical/UV photons produced in the accretion disk (e.g., Haardt & Maraschi 1991) surrounding the supermassive black hole (SMBH). The X-ray spectra of AGN are usually characterised by a continuum power law, with a photon index of  $\Gamma \sim 1.8 - 2$  (e.g., Dadina 2008, Beckmann et al. 2009, Corral et al. 2011), a soft excess at  $\lesssim 1$  keV (e.g., Turner & Pounds 1989) and reflection features arising from circumnuclear material (e.g., Matt et al. 1991). According to the classical unification scheme of AGN (Antonucci 1993) the SMBH and the accretion disk are surrounded by a molecular torus which provides anisotropic obscuration, so that Seyfert 1s (Sy1s, or type-I AGN) are observed pole-on and usually unabsorbed in the X-rays, while Seyfert 2s (Sy2s, or

type-II AGN) are seen edge-on, and usually present signatures of absorption in the X-rays. Reflection of the X-ray emission from neutral material creates a Compton hump at  $\sim 30$  keV and a fluorescent Fe  $K\alpha$  line (e.g., Lightman & White 1988). Reprocessed emission is a powerful tool to understand the geometry of the material surrounding the SMBH, and is of fundamental importance to explain the cosmic X-ray background (CXB, Giacconi et al. 1962). The spectrum of the CXB peaks at  $\sim 30$  keV (e.g., Marshall et al. 1980, Türlér et al. 2010), and the existence of a large fraction ( $\sim 30\%$ ) of Compton-thick (CT,  $N_{\text{H}} > 10^{24}$  cm $^{-2}$ ) AGN has been invoked to explain its shape (e.g., Gilli et al. 2007). This fraction is however strictly linked to the amount of reprocessed radiation assumed (Treister et al. 2009), so that larger values of the reflection parameter would imply a lower fraction of CT AGN (Gandhi et al. 2007, Ricci et al. 2011, Vasudevan et al. 2013).

The narrow component of the Fe  $K\alpha$  line peaks at 6.4 keV (e.g., Yaqoob & Padmanabhan 2004), and it has been found to be omnipresent in the X-ray spectra of local AGN (e.g.,

\* E-mail: ricci@kustastro.kyoto-u.ac.jp

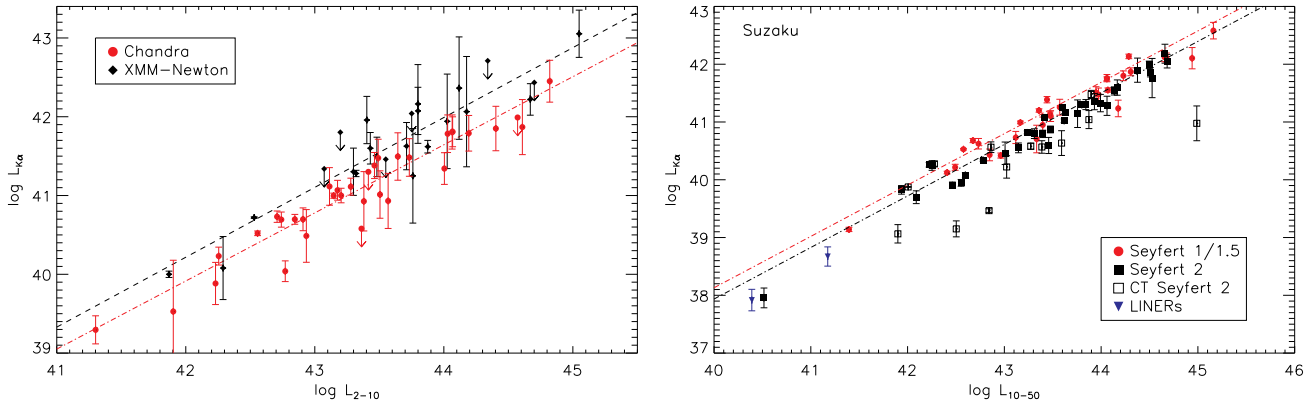


**Figure 1.** *Left panel:* Scatter plot of the iron  $K\alpha$  luminosities versus the 2–10 keV continuum luminosity of Sy1/1.5s for the *XMM-Newton* sample of Ricci et al. (2014, black diamonds) and for the *Chandra* sample of Shu et al. (2010, red circles). The black dashed and red dot-dashed line represent the best fit obtained applying Eq. 1 to the *XMM-Newton* and *Chandra* sample, respectively. *Right panel:* Scatter plot of the iron  $K\alpha$  luminosities versus the 10–50 keV absorption-corrected continuum luminosity for the *Suzaku* sample of Fukazawa et al. (2011). The red and black dot-dashed lines represent the log-linear fit (Eq. 2) for Seyfert 1s and Seyfert 2s, respectively.

Shu et al. 2012). Given its full width half maximum (FWHM) of  $\approx 2000 \text{ km s}^{-1}$  (Shu et al. 2011) this narrow component has been often associated to material located in the molecular torus (see also Ponti et al. 2013). The narrow iron  $K\alpha$  line has been found ubiquitously also in several high-redshift samples through spectral stacking: *Chandra* Deep Field North and South ( $0.5 < z < 4$ , Brusa et al. 2005), *XMM-Newton* medium survey ( $z < 3.5$ , Corral et al. 2008), *XMM-Newton* bright survey ( $z < 2.4$ , Corral et al. 2011), 2XMM catalog ( $z < 5$ , Chaudhary et al. 2012), COSMOS ( $z < 4$ , Iwasawa et al. 2012), and *XMM-Newton* observations of the *Chandra* Deep Field South ( $z < 3.5$ , Falocco et al. 2013).

The aim of this paper is to study, using the results of different works performed with *Suzaku* (Fukazawa et al. 2011), *XMM-Newton* (Ricci et al. 2014) and *Chandra* (Shu et al. 2010) data, the characteristics of the narrow Fe  $K\alpha$  line in type-I and type-II AGN. The paper is structured as follows. In Sect. 2 we study the differences in the average ratio of the Fe  $K\alpha$  and the X-ray continuum flux between type-I and Compton-thin type-II AGN, discuss the fact that contamination from the broad Fe  $K\alpha$  line is likely to be negligible in our work, and show that it can be explained by means of different average inclination angles, as foreseen by the unified model. In Sect. 3 we show that part of the Fe  $K\alpha$  flux is depleted in CT AGN, and estimate the average column density that absorbs the reflected component; in Sect. 4 we report for the first time the existence of a X-ray Baldwin effect in type-II AGN, with the same characteristics as those observed in type-I AGN. Finally, in Sect. 5 we present our conclusions. Throughout the paper we refer to Compton-thin type-II AGN as Sy2s (or type II AGN), and to CT objects as CT Sy2s.

## 2 THE FE $K\alpha$ LINE AND THE X-RAY CONTINUUM EMISSION

### 2.1 Seyfert 1s

The iron  $K\alpha$  line is created by reprocessing of the primary X-ray continuum, so that a tight correlation between the luminosity of the line and that of the continuum is expected. Fitting the data of the Sy1/1.5 *XMM-Newton* sample of Ricci et al. (2014) with a relation

of the type

$$\log L_{K\alpha} = \alpha + \beta \log L_{2-10}, \quad (1)$$

we obtained a slope of  $\beta = 0.89 \pm 0.04$ . As a comparison we fitted with Eq. 1 the *Chandra*/HEG data reported in Shu et al. (2010), and obtained a consistent slope of  $\beta = 0.86 \pm 0.01$ . In the left panel of Fig. 1 the two data sets with their respective fits are shown. The values of the Fe  $K\alpha$  EW reported in the *Chandra*/HEG study of Shu et al. (2010) are significantly lower than those obtained with *XMM-Newton*. This might be related to the higher energy resolution of *Chandra*/HEG, which makes it better suited than *XMM-Newton*/EPIC to resolve the narrow core of the line. The Fe  $K\alpha$  line detected by CCD-operating instruments like EPIC might, at least in some cases, have contributions from material located closer to the SMBH than the molecular torus, i.e. in the BLR or in the outer part of the accretion disk. Another possible source of flux is the Compton shoulder, a feature expected if the material where the line originates is Compton-thick (e.g., Matt 2002, Yaqoob & Murphy 2011). The difference in the Fe  $K\alpha$  EW measured with different instruments is also evident looking at the normalisation of the X-ray Baldwin effect reported in Table 1 of Ricci et al. (2013a): the value obtained by the *XMM-Newton*/EPIC sample of Bianchi et al. (2007) is significantly larger than that reported by the *Chandra*/HEG study of Shu et al. (2010).

### 2.2 Seyfert 1s vs Seyfert 2s

In a recent work Liu & Wang (2010), using [OIV] luminosity ( $L_{[\text{OIV}]}$ ) as a proxy for the bolometric output of AGN, found evidence of a significant difference between the Fe  $K\alpha$  luminosities of Seyfert 1s and Seyfert 2s AGN. In their work, studying *XMM-Newton* spectra, they obtained that the values of  $L_{K\alpha}$  in Compton-thin and Compton-thick Seyfert 2s are  $2.9^{+0.8}_{-0.6}$  and  $5.6^{+1.9}_{-1.4}$  times weaker than those of Seyfert 1s. Liu & Wang (2010) argued that such a difference might be due to the anisotropic emission of the Fe  $K\alpha$  line, consistently with what is expected with a line produced in the molecular torus and with the idea that Seyfert 2s are observed edge-on with respect to the torus. However, Shu et al. (2011) using the same approach and better quality *Chandra*/HEG data found only marginal differences between Seyfert 1s and Seyfert 2s.

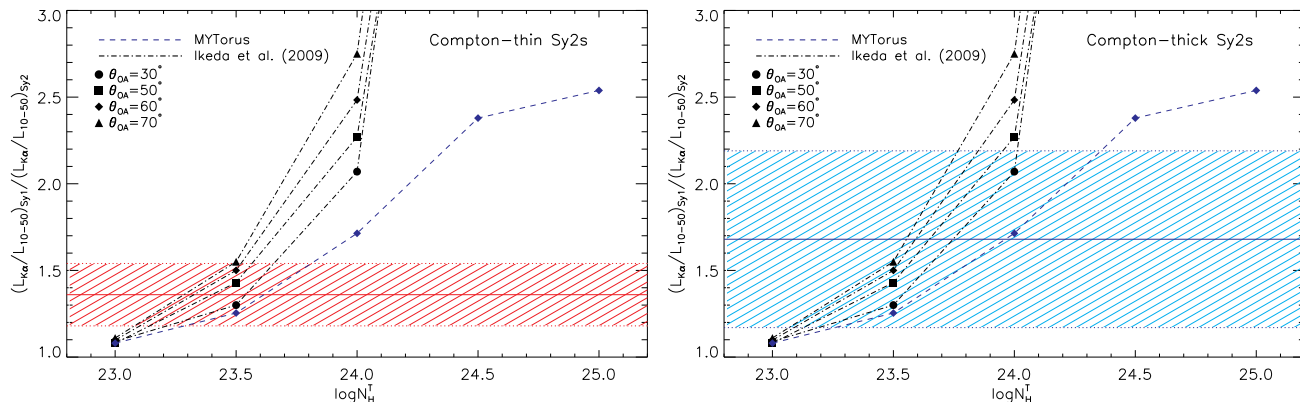


**Figure 2.** *Left panel:* average values of the ratio between the  $L_{K\alpha}/L_{10-50}$  of Sy1s and Sy2s expected for different values of the equatorial column density of the torus ( $N_{\text{H}}^{\text{T}}$ ) and of the opening angle of the torus ( $\theta_{\text{OA}}$ ). The blue dashed line represents the average values obtained simulating Sy1s and Sy2s populations using MYTorus, while the black dash-dotted line represents those obtained using the model of Ikeda et al. (2009). The red continuous line represents the average value of  $(L_{K\alpha}/L_{10-50})_{\text{Sy1}}/(L_{K\alpha}/L_{10-50})_{\text{Sy2}}$  for the Compton-thin Sy2s of the *Suzaku* sample of Fukazawa et al. (2011), while the red shaded area is its  $1\sigma$  error. *Right panel:* same as left panel, with the blue continuous line and the blue shaded area representing the average value of  $(L_{K\alpha}/L_{10-50})_{\text{Sy1}}/(L_{K\alpha}/L_{10-50})_{\text{Sy2}}$  for CT AGN and its  $1\sigma$  error, respectively.

A problem with this approach is that the relation between  $L_{\text{[OIV]}}$  and the X-ray luminosity has a large dispersion (Diamond-Stanic et al. 2009), which is bound to introduce a significant scatter in the observed  $[\text{OIV}]/\text{Fe } K\alpha$  luminosity trend.

An alternative approach to study the behaviour the Fe  $K\alpha$  luminosity in different types of AGN is to compare it to the hard X-ray ( $> 10$  keV) continuum luminosity. In the hard X-ray band photons are in fact less affected by absorption than at lower X-ray energies. In order to do so we used the results of Fukazawa et al. (2011), who carried out a large study of Fe  $K\alpha$  lines using *Suzaku* (Mitsuda et al. 2007). Of the 87<sup>1</sup> AGN reported in the work of Fukazawa et al. (2011) we excluded the seven objects for which the Fe  $K\alpha$  line was not detected and one object (NGC 4968) for which the column density  $N_{\text{H}}$  was not constrained. The final sample consists of 30 Seyfert 1s, 34 Compton-thin Seyfert 2s, 13 Compton-thick Seyfert 2s and 2 LINERs. We averaged the values of  $L_{K\alpha}$ ,  $N_{\text{H}}$ , and of the 10–50 keV luminosity of the continuum ( $L_{10-50}^{\text{obs}}$ ) for the 11 objects for which more than one observation of the same source was available. The fluxes of the X-ray continuum reported by Fukazawa et al. (2011) are not corrected for absorption. Although in the 10–50 keV band the influence of photo-electric absorption is weaker than at lower energies, Compton scattering still plays an important role, in particular for Compton-thick sources. Assuming a power-law continuum with  $\Gamma = 1.9$ , in the 10–50 keV band the observed flux is 91%, 75%, 41%, and 7% of the intrinsic value for column densities of  $\log N_{\text{H}} = 23, 23.5, 24$  and  $24.5$ , respectively.

Correcting the luminosity for absorption requires assumptions on the fraction of unabsorbed radiation reflected from material located outside the line of sight. To include self-consistently both photo-electric absorption and Compton scattering, we used MYTorus (Murphy & Yaqoob 2009) to calculate the corrections for Seyfert 2s and CT Sy2s, similarly to what was done by Burlon et al. (2011). MYTorus assumes a toroidal geometry with the half-opening angle  $\theta_{\text{OA}}$  fixed to  $60^\circ$ , and its main parameters are the photon index  $\Gamma$ , the inclination angle of the observer  $\theta_i$  and the

equatorial column density of the torus  $N_{\text{H}}^{\text{T}}$ . For each source, the corrections  $k(N_{\text{H}})$  were obtained from the ratio between the flux in the 10–50 keV band of an unabsorbed ( $\theta_i = 30^\circ$ ) and an absorbed ( $\theta_i = 90^\circ$ ) spectrum simulated using MYTorus, with  $N_{\text{H}}^{\text{T}} = N_{\text{H}}$ . The unabsorbed luminosities were then calculated multiplying the observed values by the correction ( $L_{10-50} = k(N_{\text{H}}) \times L_{10-50}^{\text{obs}}$ ). In the following we will only use the absorption-corrected 10–50 keV luminosity ( $L_{10-50}$ ). The values of  $L_{K\alpha}$  and  $L_{10-50}$  used here are reported in Appendix A.

Fitting separately the Seyfert 1s and Compton-thin Seyfert 2s *Suzaku* samples with

$$\log L_{K\alpha} = \alpha_{\text{H}} + \beta_{\text{H}} \log L_{10-50}, \quad (2)$$

we obtained  $\alpha_{\text{H},1} = 2.6 \pm 0.3$  and  $\alpha_{\text{H},2} = 2.3 \pm 0.5$ , and identical slopes  $\beta_{\text{H},1} = \beta_{\text{H},2} = 0.89 \pm 0.01$ . The fact that  $\beta < 1$  implies the existence of an anti-correlation between  $L_{K\alpha}/L_{10-50}$  and  $L_{10-50}$  (i.e., the X-ray Baldwin effect, see Sect. 4.3). In the right panel of Fig. 1, the scatter plot of  $L_{K\alpha}$  versus  $L_{10-50}$ , together with the fit for the Seyfert 1s and Seyfert 2s subsamples, is shown.

As it can be seen from Fig. 1, the average Fe  $K\alpha$  luminosity normalised to the continuum luminosity of Sy2s is lower than that of Sy1s. The mean values of  $L_{K\alpha}/L_{10-50}$  are in fact significantly different:  $0.0047 \pm 0.0004$  and  $0.0034 \pm 0.0004$  for Sy1s and Sy2s, respectively. Performing a Kolmogorov-Smirnov test we obtained a probability of 0.1% that the two distributions of  $L_{K\alpha}/L_{10-50}$  are drawn from the same parent population. In the following we discuss several possible explanations of this effect.

### 2.2.1 Different inclination angles

We tested the hypothesis that a different average inclination angle with respect to an obscuring torus between Sy1s and Sy2s, as foreseen by the unified model, could explain this difference. We created dummy Sy2 and Sy1 populations using MYTorus ( $\theta_{\text{OA}} = 60^\circ$ ) and the model of Ikeda et al. (2009), which considers a spherical-toroidal geometry with a varying half-opening angle for the reprocessing material. We adopted four different values of  $\theta_{\text{OA}}$  for the model of Ikeda et al. (2009,  $\theta_{\text{OA}} = 30^\circ, 50^\circ, 60^\circ, 70^\circ$ ), and assumed that the two populations have on average the same  $\theta_{\text{OA}}$ . The value

<sup>1</sup> In their work Fukazawa et al. (2011) report 88 AGN, but NGC 1142 and Swift J0255.2–0011 are the same source.

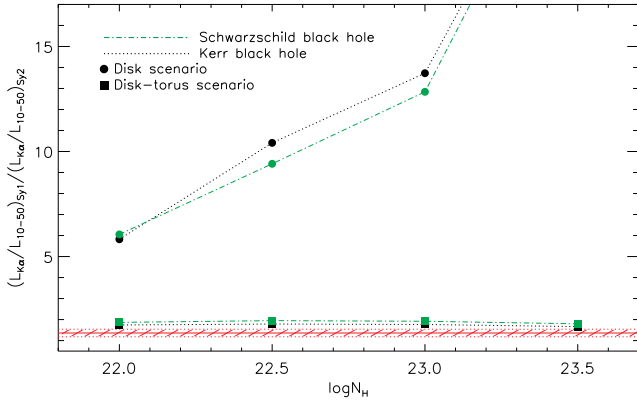


**Figure 3.** The points represent the average values of the ratio between the  $L_{K\alpha}/L_{10-50}$  of Sy1s and Sy2s expected for different values of the observed line-of-sight column density of Sy2s, assuming the Fe  $K\alpha$  line created entirely by reprocessing of the X-ray emission in the accretion disk (circles,  $R_{\text{disk}} = 1$ ), or half in the accretion disk and half in the molecular torus (squares,  $R_{\text{torus}} = R_{\text{disk}} = 0.5$ ). The values of  $L_{K\alpha}/L_{10-50}$  were calculated for a Schwarzschild (green dot-dashed line) and a Kerr black hole (dotted black line) (see Sect. 2.2.3), assuming that the inner radius of the disk corresponds to the radius of the inner stable circular orbit. The red continuous line represents the average value of  $(L_{K\alpha}/L_{10-50})_{\text{Sy1}}/(L_{K\alpha}/L_{10-50})_{\text{Sy2}}$  for the Compton-thin Sy2s of the *Suzaku* sample of Fukazawa et al. (2011), while the red shaded area is its  $1\sigma$  error.

of  $\theta_{\text{OA}}$  is thought to depend on the luminosity of the AGN (e.g., Ueda et al. 2003, see also Sect. 4.3). Performing a Kolmogorov-Smirnov test we obtained a probability of 89% that the luminosity distributions of the type-I and type-II AGN of our sample are drawn from the same parent population, which makes our assumption reasonable. We fixed  $\Gamma = 1.9$  and, for different values of  $N_{\text{H}}^{\text{T}}$ , we generated a large number of spectra with  $\theta_i$  randomly selected between  $1^\circ$  and  $\theta_{\text{OA}}$  for Sy1s, and between  $\theta_{\text{OA}}$  and  $90^\circ$  for Sy2s. We calculated the weighted average ratio between the luminosity of the Fe  $K\alpha$  line and the unabsorbed 10–50 keV luminosity, using as weights  $w = \sin \theta_i$  to take into account the probability of observing an AGN with an angle of  $\theta_i$ . In the left panel of Fig. 2, we illustrate the expected values of  $(L_{K\alpha}/L_{10-50})_{\text{Sy1}}/(L_{K\alpha}/L_{10-50})_{\text{Sy2}}$  together with the value obtained using the *Suzaku* results of Fukazawa et al. (2011). The figure shows that the difference observed between Sy1s and Sy2s can be explained by means of different average inclination angles between the two populations. The difference in the trends predicted by MYTorus and the model of Ikeda et al. (2009) are related to the different geometries considered. In the spherical-toroidal scenario the surface illuminated by the X-ray source is larger than in the case of a toroidal geometry, and a larger fraction of radiation is reflected towards a pole-on observer than in the direction of an observer located edge-on. This is responsible for the high values of  $(L_{K\alpha}/L_{10-50})_{\text{Sy1}}/(L_{K\alpha}/L_{10-50})_{\text{Sy2}}$  expected by the model of Ikeda et al. (2009) for  $\log N_{\text{H}}^{\text{T}} \geq 23.5$ .

### 2.2.2 Differences in Compton humps, abundances and photon index distributions

Ricci et al. (2011), studying the average hard X-ray (17–250 keV) spectra of AGN, found that mildly obscured Sy2s (MOB,  $23 \leq \log N_{\text{H}} < 24$ ) show a stronger Compton hump than lightly obscured objects (LOB,  $\log N_{\text{H}} \leq 23$ ). This trend was recently confirmed by stacking 14–195 keV *Swift*/BAT spectra by Vasudevan et al. (2013),

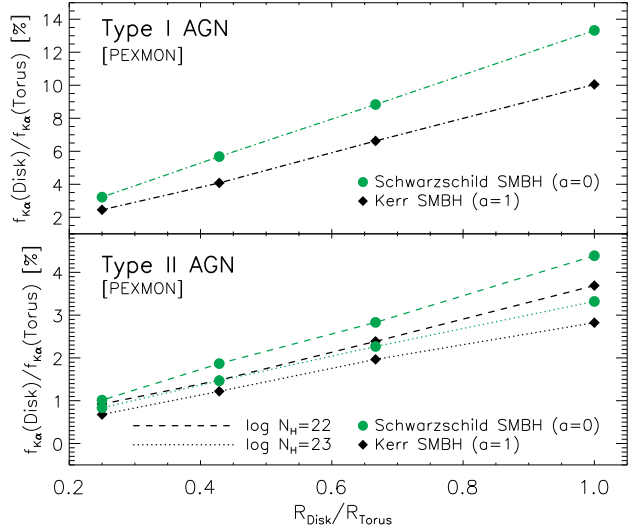


**Figure 4.** Ratio between the flux of the broad and narrow components of the Fe  $K\alpha$  in the 6.35–6.45 keV range expected for type I (top panel) and type II AGN (bottom panel), for different values of the ratio between the disk and torus reflection parameters ( $R_{\text{disk}}/R_{\text{torus}}$ ), of the line of sight column density and of the spin of the SMBH, assuming that the inner radius of the disk corresponds to the radius of the inner stable circular orbit. The model used for the disk and torus reflection is *peXmon*. The disk reflection was blurred using the *relconv* kernel.

and has been interpreted as being due to the presence of partially covering CT material in the line of sight, or to a larger covering factor of the torus in MOB Sy2s. The *Suzaku* Sy2s sample is dominated by MOB Sy2s, with only three LOB objects. Similarly to Sy1s, the three LOB AGN have an average ratio of Fe  $K\alpha$  to continuum luminosity ( $L_{K\alpha}/L_{10-50} = 0.0048$ ) larger than that of MOB Sy2s ( $L_{K\alpha}/L_{10-50} = 0.0033$ ). A larger Compton hump in MOB Sy2s would also imply larger values of  $L_{10-50}$ . This might lead to a lower  $L_{K\alpha}/L_{10-50}$  ratio for MOB Sy2s, in agreement with our results. However the relation between the Fe  $K\alpha$  line and the Compton hump luminosities depends on the origin of the enhanced reflection, so that we cannot estimate the impact of a stronger Compton hump on the differences in the values of  $L_{K\alpha}/L_{10-50}$ . Different distributions of photon indices between Sy1s and Sy2s might also explain the different distributions of  $L_{K\alpha}/L_{10-50}$ .

Another possible explanation might be the existence of differences in the iron abundances of the circumnuclear material of different classes of objects. While it not possible to fully discard this possibility, we argue that currently there is no evidence that could confirm it.

### 2.2.3 The role of broad lines

In the work of Fukazawa et al. (2011) the width of the Fe  $K\alpha$  line was not fixed. Although the lines observed were narrow ( $\sigma < 80$  eV), there might have been some contamination from the broad relativistic lines produced in the inner part of the accretion flow. Here we discuss the possibility that the differences in the  $L_{K\alpha}/L_{10-50}$  ratios between type I and type II AGN is due to the different contribution of broad lines to the observed Fe  $K\alpha$  flux in type-I and type-II AGN. Both the inclination angle and the absorbing material might play a role in decreasing the intensity of the ratio between Fe  $K\alpha$  line and the X-ray continuum luminosity in Sy2s.

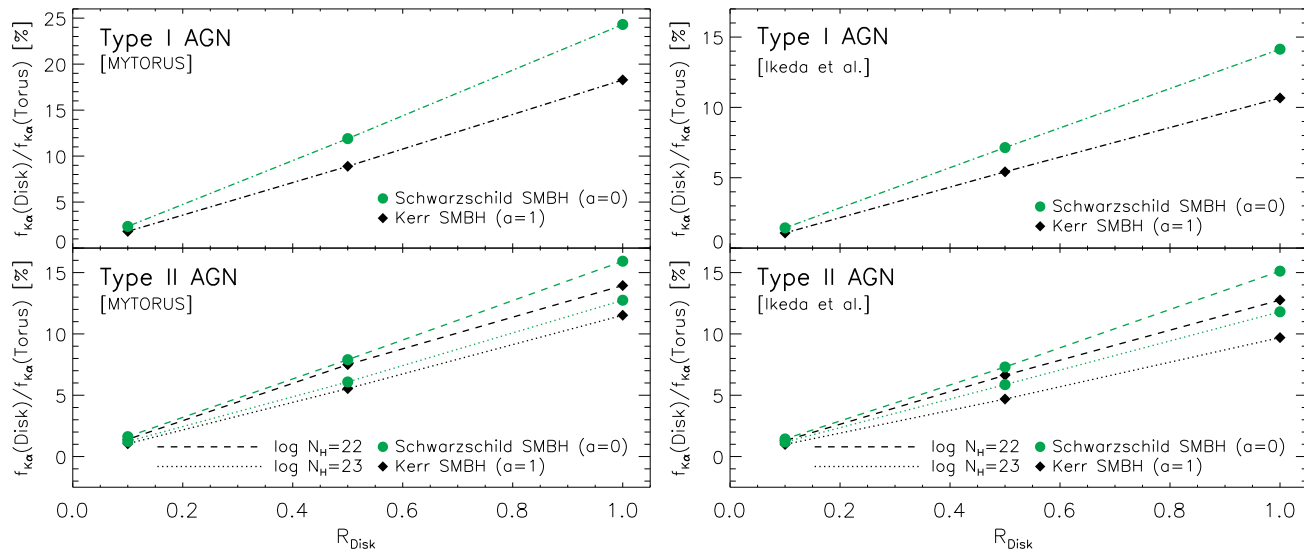


**Figure 5.** *Left panel:* Ratio between the flux of the broad and narrow components of the Fe  $K\alpha$  in the 6.35–6.45 keV range expected for type I (top panel) and type II AGN (bottom panel), for different values of the disk reflection parameter ( $R_{\text{disk}}$ ), of the line of sight column density and of the spin of the SMBH, assuming that the inner radius of the disk corresponds to the radius of the inner stable circular orbit. The model used for the blurred disk reflection is `pexmon`, convolved with the `relconv` kernel. The torus reflection was simulated using MYTORUS, fixing  $N_{\text{H}}^{\text{T}} = 10^{24} \text{ cm}^{-2}$ . *Right panel:* same as left panel using the model of Ikeda et al. (2009) to simulate the reflection from the torus (fixing  $N_{\text{H}}^{\text{T}} = 10^{24} \text{ cm}^{-2}$  and  $\theta_{\text{OA}} = 60^\circ$ ).

The absorbing material in the line of sight would in fact deplete the broad component of the Fe  $K\alpha$  line in Sy2s, while the albedo of the disk decreases for increasing values of the inclination angle of the observer.

To test the influence of broad lines we carried out extensive simulations adopting the following approach. We simulated in XSPEC spectra in the 0.3–10 keV range using a power-law continuum plus a blurred reprocessed emission, which includes a Fe  $K\alpha$  line. The X-ray reprocessed emission was accounted for using the `pexmon` model (Magdziarz & Zdziarski 1995; Nandra et al. 2007), fixing the cutoff energy to  $E_{\text{C}} = 300 \text{ keV}$ , and the value of the reflection parameter to a negative value, which allows to take into account only the reflected radiation and not the continuum. This reflected emission was then blurred using the `relconv` kernel (Dauser et al. 2010), assuming a limb-darkening law (Laor 1991). The outer radius of the accretion disk was set to  $R_{\text{out}} = 400 r_{\text{G}}$ , where  $r_{\text{G}} = GM_{\text{BH}}/c^2$  is the gravitational radius. The inclination angle with respect to the accretion disk ( $\theta_{\text{disk}}$ ) was randomly selected for each simulation in the  $1 - 60^\circ$  and  $60 - 85^\circ$  ranges for Sy1s and Sy2s, respectively. The choice of  $85^\circ$  as an upper limit is related to the limitations of `pexmon`. We tested two scenarios, one in which the spin of the SMBH is  $a = 0.998$  and the inner radius of the disk is  $R_{\text{in}} = 1.24 r_{\text{G}}$ , equivalent to a maximally-rotating Kerr black hole, and one in which  $a = 0$  and  $R_{\text{in}} = 6 r_{\text{G}}$ , as expected for a non-rotating Schwarzschild black hole. We considered four different values of the line-of-sight column density for Sy2s ( $\log N_{\text{H}} = 22, 22.5, 23$  and  $23.5$ ) for type II AGN, and took into account both photoelectric absorption (`tbabs` in XSPEC, Wilms et al. 2000) and Compton scattering (`cabs`). We fixed the internal ( $r \leq R_{\text{break}}$ ) and external ( $r > R_{\text{break}}$ ) emissivity indices to  $q_1 = q_2 = 3$ , and set the value of  $R_{\text{break}}$  to an arbitrary value. The simulated spectra were fitted using a power-law model plus a Gaussian line, with a energy fixed to 6.4 keV and a width that was left free to vary (with an upper bound of 300 eV). We calculated the weighted average ratio between the luminosity of the Fe  $K\alpha$  line

and the unabsorbed 10–50 keV luminosity, using the same weights adopted in Sect. 2.2.1 ( $w = \sin \theta_i$ ).

In Fig. 3 we illustrate the values of  $(L_{K\alpha}/L_{10-50})_{\text{Sy1}}/(L_{K\alpha}/L_{10-50})_{\text{Sy2}}$  expected for different values of  $a$  and  $N_{\text{H}}$ . We considered two cases. One in which all the emission in the Fe  $K\alpha$  band is due to blurred reflection from the disk (*disk scenario*, with a reflection parameter of  $R_{\text{disk}} = 1$ ), and one in which half of the emission is created in the disk and half in the molecular torus (*disk-torus scenario*). In the latter case we added a second unblurred `pexmon` to account for the reflection from neutral distant material ( $R_{\text{torus}} = R_{\text{disk}} = 0.5$ ), fixing the inclination angle to  $\theta_{\text{tor}} = \pi/2 - \theta_{\text{disk}}$ . This second reflection component was considered unobscured when simulating the X-ray spectra of type-II AGN. The figure shows that differences in the broad component of the Fe  $K\alpha$  line would produce a higher ratio than the one observed, both in the disk and in the disk-torus scenario, which excludes a strong influence of the broad lines in our work. If the fluxes of the Fe  $K\alpha$  lines were heavily contaminated by broad lines (disk scenario), one would expect a steep increase of the ratio  $(L_{K\alpha}/L_{10-50})_{\text{Sy1}}/(L_{K\alpha}/L_{10-50})_{\text{Sy2}}$  with the line-of-sight column density for  $\log N_{\text{H}} \geq 23$ . This is not observed (see Fig. 6 and Sect. 3). A scenario in which reflection from the disk and from the torus have the same influence could also be discarded, as it would lead to values of  $(L_{K\alpha}/L_{10-50})_{\text{Sy1}}/(L_{K\alpha}/L_{10-50})_{\text{Sy2}}$  higher than the observed ones. This implies that on average  $R_{\text{disk}}/R_{\text{torus}} < 1$ .

To estimate the ratio between the flux of broad and narrow Fe  $K\alpha$  lines at 6.4 keV we simulated two sets of dummy AGN populations, taking into account only reflection and considering  $R_{\text{disk}}/R_{\text{torus}} < 1$ . One set of spectra were simulated using blurred reflection (`relconv` (`pexmon`) in XSPEC), while the other considering unblurred reflection (`pexmon`). We considered two different scenarios to study the ratio in type I and type II AGN. For type I AGN we randomly selected inclination angles in the  $1 - 60^\circ$  and  $30 - 85^\circ$  ranges for the blurred and unblurred reflection component, respectively. We then obtained the fluxes for each simulated spectrum in

the 6.35–6.45 keV range, and calculated the weighted averages for the blurred and unblurred reflection case, using the same weights adopted in Sect. 2.2.1. In Fig. 4 (top panel) we illustrate the values of the ratio between the 6.35–6.45 keV fluxes of broad and narrow lines ( $f_{K\alpha}(\text{disk})/f_{K\alpha}(\text{torus})$ ) for different values of  $R_{\text{disk}}/R_{\text{torus}}$ , and considering a disk accreting onto a Schwarzschild or a maximally rotating Kerr black hole. For type II AGN we followed the same approach used for type I, including absorption in the case of the blurred reflection<sup>2</sup>, and selecting random angles in the 60 – 85° and 5 – 30° ranges for the blurred and unblurred reflection component, respectively. As shown in Fig. 4, for type I AGN we obtained  $f_{K\alpha}(\text{disk})/f_{K\alpha}(\text{torus}) < 14\%$ , while for type II AGN the influence of the broad line is even lower ( $f_{K\alpha}(\text{disk})/f_{K\alpha}(\text{torus}) < 5\%$ ). The values of the ratios obtained using MYTORUS and the model of Ikeda et al. (2009) instead of pexmon to simulate the reflection from the torus are shown in Fig. 5. In both models the equatorial column density of the torus was fixed to  $N_{\text{H}}^{\text{T}} = 10^{24} \text{ cm}^{-2}$ , and in the model of Ikeda et al. (2009) the half-opening angle of the torus was set to  $\theta_{\text{OA}} = 60^\circ$ . The values of the  $f_{K\alpha}(\text{disk})/f_{K\alpha}(\text{torus})$  ratios are  $< 25\%$  for type I AGN, and  $< 15\%$  for type II AGN<sup>3</sup>. These simulations show that the influence of disk lines is on average marginal in our work.

Further evidence that the broad Fe K $\alpha$  line does not play a significant role in our work comes from the fact that the width of the lines does not decrease with increasing values of  $N_{\text{H}}$ , and the mean width of the Fe K $\alpha$  line obtained for different AGN classes are consistent:  $\sigma_{\text{Sy}1} = 79 \text{ eV}$  and  $\sigma_{\text{Sy}2} = 64 \text{ eV}$ , with a standard deviation of 37 and 33 eV, respectively. Our simulations show that significant differences in the width of the Fe K $\alpha$  line between type I and type II AGN are expected if the disk reflection is as strong as the torus reflection. The idea that the contribution of broad lines to our work is marginal is also supported by the fact that the values of  $\sigma$  are much smaller than those obtained by Patrick et al. (2012) ( $\sigma \approx 500 \text{ eV}$ ) studying relativistic disk lines using *Suzaku*, and by the fact that the energy of the Gaussian lines reported by Fukazawa et al. (2011) is on average  $E = 6.399 \text{ keV}$ , a value in good agreement with neutral or low-ionisation Fe K $\alpha$  fluorescent emission.

### 3 ABSORPTION OF REPROCESSED EMISSION

In the  $\log L_{K\alpha} - \log L_{10-50}$  plane, CT Sy2s have a significantly flatter slope ( $\beta_{\text{H,CT}} = 0.36 \pm 0.02$ ) than Sy1s and Sy2s, and as shown in Fig. 1 (right panel) their Fe K $\alpha$  luminosity is systematically lower than that observed in Sy1s and Sy2s for the same continuum luminosity. We tested the idea that this difference could be explained in terms of different inclination angles. Comparing the ratios of the Fe K $\alpha$  and the continuum luminosities of CT Sy2s and Sy1s we obtained an average value of  $(L_{K\alpha}/L_{10-50})_{\text{Sy}1}/(L_{K\alpha}/L_{10-50})_{\text{CT}} = 1.68 \pm 0.51$ , consistent with the theoretical predictions for a toroidal structure of the reprocessing and absorbing material, but not for a spherical-toroidal geometry (see right panel of Fig. 2), because  $N_{\text{H}}^{\text{T}}$  cannot be lower than  $N_{\text{H}}$ .

An alternative explanation is that in these objects part of the reflected radiation is absorbed. Plotting the  $L_{K\alpha}/L_{10-50}$  ratio versus the observed column density (Fig. 6), we found a steep decrease of

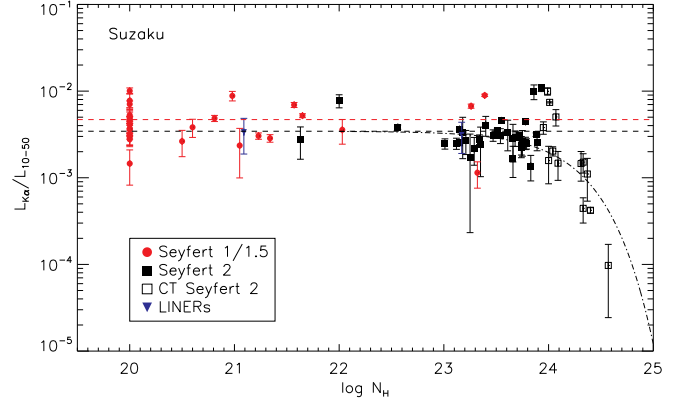


**Figure 6.** Ratio between the Fe K $\alpha$  and the continuum luminosity ( $L_{K\alpha}/L_{10-50}$ ) versus the observed hydrogen column density ( $N_{\text{H}}$ ) for the *Suzaku* sample of Fukazawa et al. (2011). The continuum luminosities were corrected to account for photoelectric absorption and Compton scattering as described in Sect. 2.2. The unabsorbed objects were arbitrarily assigned  $\log N_{\text{H}} = 20$ . The red and black dashed lines represent the average of the ratio  $L_{K\alpha}/L_{10-50}$  for Seyfert 1s and Seyfert 2s, respectively. The dot-dashed black line represents the best fit to the Sy2s and CT Sy2s data obtained using Eq. 4.

the relative iron K $\alpha$  emission above  $N_{\text{H}} \sim 10^{24} \text{ cm}^{-2}$ . Fitting this decrease (for  $\log N_{\text{H}} \geq 24$ ) with a log-linear relation we obtained

$$\log \frac{L_{K\alpha}}{L_{10-50}} = (-3.12 \pm 0.08) \log N_{\text{H},22} + (4.1 \pm 0.2), \quad (3)$$

where  $N_{\text{H},22}$  is the column density in units of  $10^{22} \text{ cm}^{-2}$ . No significant trend is found in Seyfert 2s (with a null hypothesis probability of  $P_n \approx 99\%$ ). The decrease of  $L_{K\alpha}/L_{10-50}$  with the observed column density in CT Sy2s is likely to be due to absorption of the reflected emission from the material located between the observer and the X-ray source, often associated to the putative molecular torus. A similar decrease is also found using the time-averaged absorption-corrected 14–195 keV *Swift*/BAT luminosities (Baumgartner et al. 2010, see Sect. 4.2) instead of the 10–50 keV *Suzaku* luminosities.

From the decrease of  $L_{K\alpha}/L_{10-50}$  with  $N_{\text{H}}$  it is possible to obtain the average fraction of the line-of-sight column density that absorbs the X-ray radiation reprocessed in the molecular torus ( $X_{\text{R}}$ ). This can be done by fitting the data of Sy2s and CT Sy2s with the following relation:

$$\frac{L_{K\alpha}}{L_{10-50}} = \frac{L_{K\alpha}^{\text{unabs}}}{L_{10-50}} \times \exp\{-[\sigma_{\text{T}} + \sigma_{\text{ph}}(6.4 \text{ keV})] \times X_{\text{R}} \times N_{\text{H}}\}, \quad (4)$$

where  $L_{K\alpha}^{\text{unabs}}$  is the unabsorbed luminosity of the Fe K $\alpha$  line,  $\sigma_{\text{T}}$  is the Thomson cross section, and  $\sigma_{\text{ph}}(6.4 \text{ keV})$  is the photoelectric cross section at 6.4 keV. The value of  $\sigma_{\text{ph}}$  at 6.4 keV was calculated using the coefficients of the analytic fit in the 4.038–7.111 keV energy band reported by Morrison & McCammon (1983). We fixed  $L_{K\alpha}^{\text{unabs}}/L_{10-50}$  to the ratio obtained for Sy2s, as this value is constant up to  $\log N_{\text{H}} \sim 24$ . From the fit we obtained  $X_{\text{R}} = 0.24 \pm 0.01$ , which implies that on average the reflected emission is absorbed by a column density which is about 1/4 of the one that absorbs the X-ray primary emission.

It should be remarked that Fukazawa et al. (2011) report values of the column density of  $\log N_{\text{H}} \sim 24$  for two objects, NGC 1068 and ESO 323–G032, which have been reported by other works as being reflection-dominated, with column densities of

<sup>2</sup> `tbabsxcabs[relconv(pexmon)]`

<sup>3</sup> The relative influence of the disc line would however increase if the disc is truncated or in the presence of light bending (e.g. Miniutti & Fabian 2004)

**Table 1.** Intercept ( $\alpha$ ), slope ( $\beta$ ), and Spearman’s rank coefficient ( $\rho$ ) obtained by fitting  $L_{K\alpha}$  and the MIR luminosities of the *Suzaku* sample of Fukazawa et al. (2011) with Eq. 5 for the different subsamples. The MIR luminosities in the  $3.4\ \mu\text{m}$  (1, 2, 3),  $4.6\ \mu\text{m}$  (4, 5, 6),  $12\ \mu\text{m}$  (7, 8, 9), and  $22\ \mu\text{m}$  (10, 11, 12) band were taken from the *WISE* all-sky survey.

Sample	$3.4\ \mu\text{m}$			$4.6\ \mu\text{m}$			$12\ \mu\text{m}$			$22\ \mu\text{m}$		
	(1)	(2)	(3)	(4)	(5)	(6)	(7)	(8)	(9)	(10)	(11)	(12)
	$\alpha_{\text{MIR}}$	$\beta_{\text{MIR}}$	$\rho$									
Seyfert 1s	$41.04 \pm 0.01$	$1.05 \pm 0.01$	0.94	$41.08 \pm 0.01$	$1.00 \pm 0.01$	0.94	$41.06 \pm 0.01$	$1.10 \pm 0.01$	0.94	$40.93 \pm 0.01$	$1.14 \pm 0.01$	0.87
Seyfert 2s	$41.16 \pm 0.01$	$0.96 \pm 0.02$	0.80	$41.18 \pm 0.01$	$0.92 \pm 0.02$	0.79	$41.09 \pm 0.01$	$0.95 \pm 0.02$	0.75	$40.88 \pm 0.01$	$0.82 \pm 0.02$	0.69
CT Seyfert 2s	$40.08 \pm 0.01$	$0.52 \pm 0.03$	0.76	$39.99 \pm 0.01$	$0.38 \pm 0.02$	0.76	$39.83 \pm 0.01$	$0.24 \pm 0.02$	0.63	$39.84 \pm 0.01$	$0.47 \pm 0.03$	0.75
Sy1s + Sy2s	$41.10 \pm 0.01$	$1.00 \pm 0.01$	0.84	$41.13 \pm 0.01$	$0.96 \pm 0.01$	0.85	$41.08 \pm 0.01$	$1.04 \pm 0.01$	0.84	$40.91 \pm 0.01$	$1.02 \pm 0.01$	0.80

$\log N_{\text{H}} \geq 25$  (Matt et al. 1997; Comastri et al. 2010). Interestingly, these two objects have a value of  $L_{K\alpha}/L_{10-50}$  significantly larger than the average value (Fig. 6), which is probably related to the under-estimation of the intrinsic luminosity due to the low value of  $N_{\text{H}}$  reported by Fukazawa et al. (2011).

The technique we used to correct the continuum luminosity for absorption is geometry-dependent, and takes into account also reflection from the torus. Correcting the values of the luminosity taking into account only the X-ray primary emission, and thus excluding the reflected flux, results in an even steeper decrease of  $L_{K\alpha}/L_{10-50}$  with  $N_{\text{H}}$  for CT AGN. An alternative approach is to compare the Fe  $K\alpha$  luminosity of AGN to their MIR luminosities, as the emission in this band is produced by the material responsible for the flux attenuation and thus expected to be less biased by absorption (e.g., Ichikawa et al. 2012). This was done cross-correlating the *Suzaku* sample with the *WISE* all-sky survey catalog (Wright et al. 2010). Of the 79 objects of the *Suzaku* sample, only for the Seyfert 2 Mrk 3 no flux is reported in the *WISE* all-sky source catalog. The MIR luminosities reported in the *WISE* catalog are in the  $3.4\ \mu\text{m}$ ,  $4.6\ \mu\text{m}$ ,  $12\ \mu\text{m}$ ,  $22\ \mu\text{m}$  band. We considered photometric values obtained by PSF-fitting, and for each of the four bands we performed a fit using

$$\log L_{K\alpha} = \alpha_{\text{MIR}} + \beta_{\text{MIR}} \log L_{\text{MIR}, 43.5}, \quad (5)$$

where  $L_{\text{MIR}, 43.5}$  is the luminosity in units of  $10^{43.5}\ \text{erg s}^{-1}$ . The results of the fits are reported in Table 1 for the different AGN subsamples. In Fig. 7 we show the scatter plot of  $L_{K\alpha}$  versus the  $12\ \mu\text{m}$  luminosity. The scatter in the correlation is larger than the one observed comparing  $L_{K\alpha}$  to  $L_{10-50}$ , but it still shows that Compton-thick sources have a lower Fe  $K\alpha$  luminosity than Compton-thin Seyfert 2s and Seyfert 1s. Some of the scatter in the correlation might be related to contamination from the host galaxy, as the spatial resolution of *WISE* does not allow to clearly discern the emission of material located close to the central engine from that of dust on the kpc scale. Another source of scatter might be the different covering factors and equatorial column densities of the tori. Of the four bands, the  $3.4\ \mu\text{m}$  and  $22\ \mu\text{m}$  are the most affected by host galaxy contamination, while the  $3.4\ \mu\text{m}$  and  $4.6\ \mu\text{m}$  band could be subject to contamination from PAH. Using high spatial resolution photometry, Gandhi et al. (2009) have shown that the intrinsic MIR emission of CT Sy2s is not significantly affected by absorption. Moreover, significant absorption would imply that the MIR luminosity of CT AGN is larger than that reported by *WISE*. This would move rightward the CT sources in Fig. 7, resulting in a Fe  $K\alpha$  luminosity even lower than the observed one when compared to Seyfert 1s and Seyfert 2s.

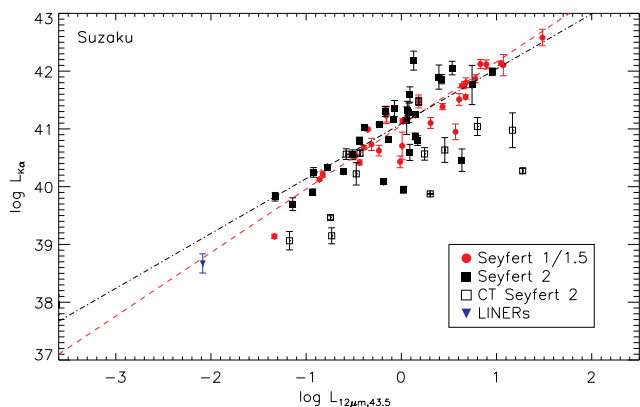


**Figure 7.** Fe  $K\alpha$  luminosities versus the  $12\ \mu\text{m}$  band luminosities (in units of  $10^{43.5}\ \text{erg s}^{-1}$ ) for the *Suzaku* sample of Fukazawa et al. (2011). The MIR luminosities were taken from the *WISE* all sky survey. The red dashed and the black dot-dashed lines represent the fits obtained using Eq. 5 for Seyfert 1s and Seyfert 2s, respectively (see also Table 1).

The fits obtained applying Eq. 5 show that CT AGN have a significantly flatter slope, and that for the same MIR luminosity their Fe  $K\alpha$  luminosities are systematically lower than those of Seyfert 1s and Seyfert 2s in the four bands for which *WISE* observations were available. This confirms the idea that in very obscured objects part of the reflected component is absorbed, and it should be taken into account when carrying out spectroscopical X-ray analysis and studies of their luminosity function. These findings should also have important consequences on synthesis models of the CXB. Absorption of part of the reflected flux would in fact imply that a larger number of CT AGN is needed. In a future work we will estimate how the fraction of CT AGN would change because of the absorption of the reprocessed radiation.

## 4 THE X-RAY BALDWIN EFFECT

### 4.1 Seyfert 1s and Seyfert 2s

The existence of a significant anti-correlation between EW and  $L_{2-10}$  (i.e. the X-ray Baldwin effect, Iwasawa & Taniguchi 1993) has been confirmed in the last years by several works carried out with the highest energy resolution available in the X-rays (e.g., Bianchi et al. 2007, Shu et al. 2010). To study the relation between Fe  $K\alpha$  EW and  $L_{2-10}$  for the *XMM-Newton* sample of type-I AGN

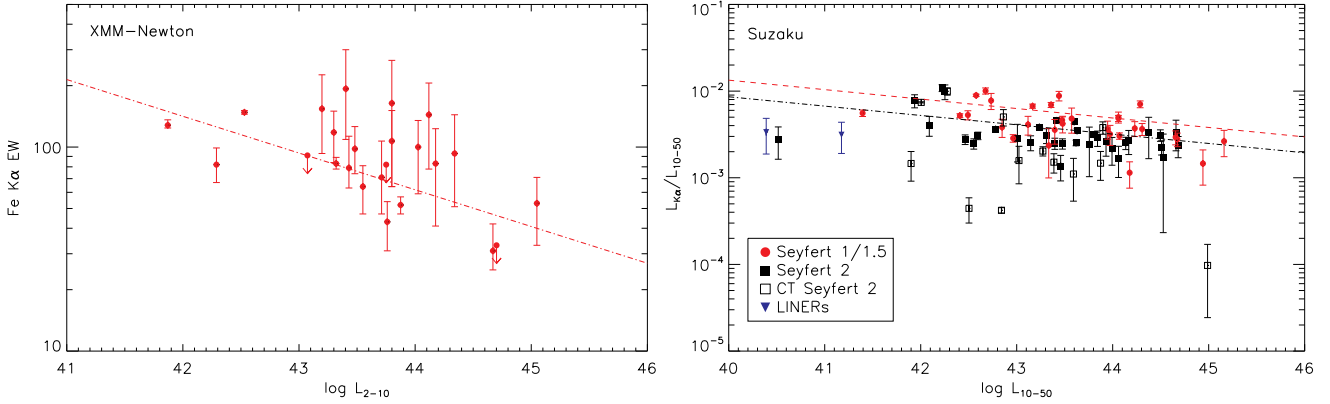


**Figure 8.** *Left panel:* Fe  $K\alpha$  EW versus the continuum luminosity for the *XMM-Newton* sample of Sy1s of Ricci et al. (2014). The red dashed line represents the fit (with a slope of  $\bar{\mu} = -0.16 \pm 0.06$ ) to the data obtained using the regression method for left censoring data described in Sect. 4.1. *Right panel:* ratio between the luminosity of the Fe  $K\alpha$  and that of the 10–50 keV continuum ( $L_{K\alpha}/L_{10-50}$ ) versus  $L_{10-50}$  for the *Suzaku* sample of Fukazawa et al. (2011). The values of  $L_{10-50}$  of Sy2s and Compton-thick Seyfert 2s have been corrected for absorption as described in Sect. 2. The red (black) dashed (dot-dashed) line represents the best fit to the data obtained using Eq. 7 for Sy1s (Sy2s). The Sy1 and Sy2 sample have the same slope ( $\omega_1 = \omega_2 = -0.11 \pm 0.01$ ).

of Ricci et al. (2014), which includes several upper limits, we follow what was done by Guainazzi et al. (2006) using the regression method for left censoring data (Schmitt 1985, Isobe et al. 1986). We carry out 10,000 Monte-Carlo simulations based on the results of the observations, applying the two following requirements: i) for the detections we substitute the values of the Fe  $K\alpha$  EW with a random Gaussian distribution, in which the mean is the value obtained by the fit, and the standard deviation its error; ii) for the upper limits U we use a random uniform distribution in the interval  $[0, U]$ . For each Monte-Carlo run we fit the values with a log-linear relationship of the type

$$\log EW = \lambda + \mu \log L_{2-10}. \quad (6)$$

We obtain an average slope  $\bar{\mu} = -0.18 \pm 0.06$ , a value consistent with the results obtained by the recent studies of Shu et al. (2010,  $\mu = -0.13 \pm 0.04$ ) and Shu et al. (2012,  $\mu = -0.11 \pm 0.03$ ). In Fig. 8 (left panel) we show the  $EW - L_{2-10}$  scatter plot for our sample together with the best fit to the data.

An alternative approach to study the X-ray Baldwin effect is to use the ratio between the line and the continuum luminosity (i.e.,  $L_{K\alpha}/L_{10-50}$ ) as a proxy of the EW. This allows to correct for the effects of absorption and to extend the study of the X-ray Baldwin effect to Seyfert 2s. While the existence of a decrease of the relative flux of the Fe  $K\alpha$  line with the luminosity has been found in several samples of Seyfert 1s, studies of Seyfert 2s have always taken into account the EW of the line, which is significantly enhanced for absorbed objects due to the damping of the continuum at  $\sim 6 - 7$  keV. We fit the *Suzaku* values of the different samples of Seyfert galaxies with the log-linear relation

$$\log \left( \frac{L_{K\alpha}}{L_{10-50}} \right) = \phi + \omega \log L_{10-50}. \quad (7)$$

To remove any bias introduced by absorption on the continuum luminosities of CT Sy2s and Sy2s, we use the same corrections applied in Sect. 2. We find that the anti-correlation is statistically significant for both the Sy1s and Sy2s sample. For Sy1s we obtain a null hypothesis probability of  $P_n \approx 0.2\%$  and a slope of  $\omega_1 = -0.11 \pm 0.01$ . For Sy2s we find  $P_n \approx 1\%$  and  $\omega_2 = -0.11 \pm 0.01$ . To our knowledge this is the first statistically significant detection of the X-ray Baldwin effect in Seyfert 2s. The fact that the slopes of

Sy1s and Sy2s are the same is a strong indication that the mechanism responsible for the decrease of the relative flux of the iron  $K\alpha$  line with the luminosity is the same. No significant trend is found considering only the sample of CT Sy2s. This is probably related to the absorption of part of the Fe  $K\alpha$  flux, as demonstrated in Sect. 3, which is bound to hide the anti-correlation. We tested whether the presence of radio-loud AGN might play a role in the correlation, and fitted the data excluding the four radio-loud type-I AGN, and the five radio-loud type-II. We found results in agreement with those obtained including these sources. In particular the slopes obtained are  $\omega_1 = -0.09 \pm 0.01$  ( $P_n \approx 1.8\%$ ) and  $\omega_2 = -0.14 \pm 0.02$  ( $P_n \approx 1.6\%$ ) for Sy1s and Sy2s, respectively.

## 4.2 Comparison with time-averaged *Swift*/BAT data

In order to reduce the possible effects of variability on the X-ray Baldwin effect, we combined the Fe  $K\alpha$  luminosities of the *Suzaku* sample (Fukazawa et al. 2011) with 58-months averaged 14–195 keV luminosity reported in the *Swift*/BAT catalog (Baumgartner et al. 2010). We excluded the three sources not detected by *Swift*/BAT and the low-luminosity type-II AGN NGC 4395, so that the final sample contained 30 Seyfert 1s and 30 Compton-thin Seyfert 2s. As proxy of the Fe  $K\alpha$  EW we used the ratio between the luminosity of the Fe  $K\alpha$  line and that of the 14–195 keV continuum ( $L_{BAT}$ ). We did not find any statistically significant anti-correlation between the  $L_{K\alpha}/L_{BAT}$  and  $L_{BAT}$ . However, given the larger energy range of the BAT luminosities, the spread in photon indices might introduce a large scatter, and thus wash out the intrinsic trend. To remove any possible dependency of the luminosity on  $\Gamma$  we calculated for each source, using the BAT photon indices, the monochromatic luminosity at 7.1 keV. Using  $L_{7.1\text{keV}}$  instead of  $L_{BAT}$  we find an anti-correlation with slopes consistent, for both Sy1s ( $\omega_1 = -0.12 \pm 0.04$ ) and Sy2s ( $\omega_2 = -0.08 \pm 0.04$ ), with those obtained using *Suzaku* luminosities (Sect. 4.1), albeit with a larger scatter. This shows that variability does not play an important role in the anti-correlation.

In Fig. 9 we illustrate the scatter plot of the the 10–50 keV *Suzaku* luminosity versus the 14–195 keV *Swift*/BAT luminosity. Performing a linear fit of the type  $\log L_{10-50} \propto K \cdot \log L_{14-195}$  on the data, we obtained  $K = 1.04 \pm 0.02$ . The scatter in the correlation is

mostly due to variability, and is similar in the two classes of objects: the standard deviation from the fit is of  $\sigma = 0.16$  and  $\sigma = 0.14$  for Sy1s and Sy2s, respectively.

### 4.3 Explaining the anti-correlation

Several explanations to the X-ray Baldwin effect have been put forward since its discovery. Nandra et al. (1997) and Nayakshin (2000) discussed how a luminosity-dependent ionisation state of the material where the line is produced might create the observed  $EW - L_{2-10}$  trend. Their models assumed that the Fe  $K\alpha$  line is produced in the disk, but a similar scenario could be imagined for material located in the BLR or in the molecular torus. A luminosity-dependent ionisation state would imply a larger flux of ionised (H and He-like, e.g., Matt et al. 1996) iron relative to neutral iron at high luminosities. However, Bianchi et al. (2007) using a large sample of type-I AGN observed with *XMM-Newton* found only a weak statistically non-significant correlation between the ratio of the flux of ionised and neutral iron ( $F(\text{Fe XXV} + \text{Fe XXVI})/F(\text{Fe I})$ ) and the X-ray luminosity.

Jiménez-Bailón et al. (2005) and Jiang et al. (2006) argued that the correlation might be driven by the presence of radio-loud objects. However several recent works have showed that a significant correlation is also found when considering only radio-quiet AGN (e.g., Bianchi et al. 2007, Shu et al. 2010). Moreover, evidence of an X-ray Baldwin effect in radio-loud AGN has been found by Grandi et al. (2006) using *BeppoSAX* observations.

Jiang et al. (2006) proposed that the non-simultaneous reaction of the reprocessing material responsible for the Fe  $K\alpha$  line to flux changes of the continuum might cause the trend. Given the distance of the torus from the X-ray source and its size, the line is in fact expected to react on much longer time-scales to flux changes of the continuum emission. This effect was investigated by Shu et al. (2010), who found that X-ray variability might cause at least part of the correlation, and that averaging different observations of the same source the slope of the X-ray Baldwin effect is flatter ( $\mu = -0.13 \pm 0.04$ ) than the one obtained using all the observations ( $\mu = -0.22 \pm 0.03$ , see also Table 1 in Ricci et al. 2013a). Another proof of the importance of variability was found by Shu et al. (2012), who detected a clear  $EW - L_{2-10}$  anti-correlation for individual sources. However, Shu et al. (2012) carrying out simulations in which the X-ray continuum is variable and the Fe  $K\alpha$  line is constant, found that variability cannot account for the whole X-ray Baldwin effect. Moreover, in Section 4.2 we have shown that, using X-ray luminosities averaged over several years, we still find evidence of an X-ray Baldwin effect both in Sy1s and Sy2s.

It has been shown that the Fe  $K\alpha$  EW decreases with the Eddington ratio ( $\lambda_{\text{Edd}}$ ) with a slope similar to that obtained using the X-ray luminosity (e.g., Bianchi et al. 2007). This leads to the possibility that the X-ray Baldwin effect might be related to the known relation between the photon index of the continuum power-law spectrum and the Eddington ratio (e.g., Shemmer et al. 2008). The fact that for higher values of the Eddington ratio the photon index is steeper implies a lower number of photons at the energy of the Fe  $K\alpha$  line, which leads to lower values of EW. In a recent paper (Ricci et al. 2013b) we have carried out simulations to study the impact of this trend considering three different geometries of the reflecting material (toroidal, spherical toroidal and slab). We found that considering the  $\Gamma - \lambda_{\text{Edd}}$  relation obtained by Shemmer et al. (2008;  $\Gamma \propto 0.31 \log \lambda_{\text{Edd}}$ ) one would obtain at most a slope of  $\sim -0.08$ , lower than the value found using the *Chandra*/HEG data of Shu et al. (2010;  $\log EW \propto (-0.13 \pm 0.03) \log \lambda_{\text{Edd}}$ ). A slope con-

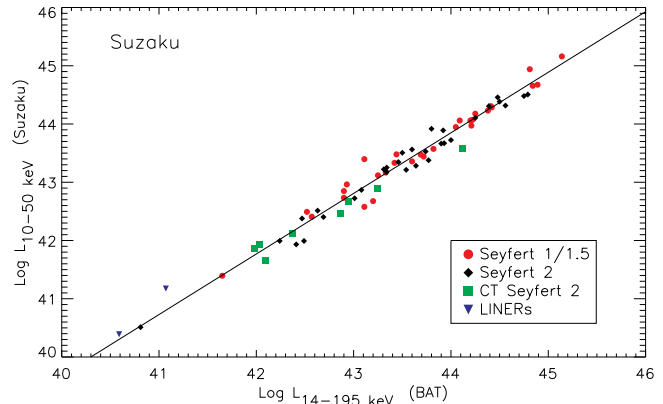


**Figure 9.** Scatter plot of the 10–50 keV *Suzaku* luminosity versus the 14–195 keV *Swift*/BAT luminosity. The continuous line represents the best linear fit to the data, with a slope of  $K = 1.04 \pm 0.2$ .

sistent with the observations would be produced using the results of Risaliti et al. (2009) and Jin et al. (2012), who found a steeper increase of  $\Gamma$  with  $\lambda_{\text{Edd}}$  ( $\Gamma \propto 0.58 \log \lambda_{\text{Edd}}$ ) than previous works. If the  $\Gamma - \lambda_{\text{Edd}}$  correlation is responsible for the X-ray Baldwin effect, then our results imply that the link between the X-ray corona and the accretion flow is similar in Sy1s and Sy2s.

A decrease of the fraction of obscured objects ( $f_{\text{obs}}$ ) with the luminosity has been observed in a very large number of surveys, from the radio to the hard X-rays (e.g., Grimes et al. 2004, Maiolino et al. 2007, Simpson 2005, Beckmann et al. 2009). This phenomenon is often explained, in the framework of luminosity-dependent unification models, by the decrease of the covering factor of the torus with the luminosity, possibly caused by the effect of radiation pressure on the dust and gas of the torus. Because of the strong dependence of the Fe  $K\alpha$  EW on the covering factor of the torus (e.g., Ikeda et al. 2009), this mechanism has been often invoked as a possible explanation for the X-ray Baldwin effect (e.g., Page et al. 2004, Zhou & Wang 2005). In a recent work (Ricci et al. 2013a), we have used physical torus models and recent X-ray and IR measurements of the decrease of  $f_{\text{obs}}$  with the luminosity to quantify the effect of this phenomenon on the Fe  $K\alpha$  EW. We found that in the Seyfert regime ( $42 \leq \log L_{2-10} \leq 44.2$ ) luminosity-dependent unification can reproduce the slope of the X-ray Baldwin effect for a large range of values of equatorial column densities of the torus ( $\log N_{\text{H}}^{\text{T}} \geq 23.1$ ). In the quasar regime ( $\log L_{2-10} > 44.2$ ) the situation is less clear, due to the smaller sample and to the large errors associated to the values of the Fe  $K\alpha$  EW, but our results seem to indicate that a slower decrease of  $f_{\text{obs}}$  with  $L_{2-10}$  than that observed at lower luminosities is necessary to explain the observations. In the Seyfert regime the intercept of the X-ray Baldwin effect found by *Chandra*/HEG observations (Shu et al. 2010) can be explained only by a torus with an equatorial column density of  $\log N_{\text{H}}^{\text{T}} \approx 23.2$ . This value is lower than the  $N_{\text{H}}$  observed in many Sy2s, and might be related to the fact that the spherical-toroidal geometry we used is expected to produce values of EW larger than a toroidal geometry for the same set of parameters. If the decrease of the covering factor of the torus with the luminosity is the cause of the X-ray Baldwin effect, our findings show that on average the tori of Sy2s behave similarly to those of Sy1s.

Amongst the different explanations proposed for the X-ray Baldwin effect, so far luminosity-dependent unification seems to be the most promising. The effect of the  $\Gamma - \lambda_{\text{Edd}}$  trend would also

be able to account for the observed  $EW - L_{2-10}$  relation, but only for a steep increase of  $\Gamma$  with  $\lambda_{\text{Edd}}$ , which has yet to be confirmed. In order to discern between these two explanations it is necessary to understand whether the main driver of the X-ray Baldwin effect is the luminosity or the Eddington ratio. In Ricci et al. (2013b) we show that the  $EW - L_{2-10}$  anti-correlation is statistically more significant than the  $EW - \lambda_{\text{Edd}}$  one. However uncertainties on the estimates of the black hole masses and on the bolometric corrections do not allow to fully discard the possibility that  $\lambda_{\text{Edd}}$  is the main driver of the X-ray Baldwin effect.

## 5 SUMMARY AND CONCLUSIONS

In this work, we studied the relation between the narrow Fe  $K\alpha$  line and the X-ray continuum in different types of AGN, using the results of several X-ray works carried out using *Chandra*, *XMM-Newton*, and *Suzaku*. Our main results are the following.

- The luminosity of the Fe  $K\alpha$  line normalised to that of the continuum is on average lower in Sy2s than in Sy1s (right panel of Fig. 1). Studying the average values of  $L_{K\alpha}/L_{10-50}$  obtained simulating dummy Sy1s and Sy2s populations, we showed that this difference is consistent with being due to different average inclination angles with respect to the molecular torus (left panel of Fig. 2), confirming the existence of an axisymmetric structure (torus-like) responsible for the reprocessing of the X-ray radiation. Alternatively, this difference might be due to differences in the intensities of Compton humps, in the photon index distributions or in the average iron abundances.

- We showed that the ratio between the flux of the broad and narrow Fe  $K\alpha$  line in the 6.35–6.45 keV range depends on the torus geometry considered, and is on average  $< 25\%$  and  $< 15\%$  for type I and type II AGN, respectively (see Figs. 4 and 5).

- We showed that the luminosity of the Fe  $K\alpha$  line is attenuated in CT Sy2s (Fig. 6) due to absorption of part of the reflected component. This result is also confirmed comparing the  $L_{K\alpha}$  of the AGN to their MIR luminosity (Fig. 7 and Table 1), which shows that the luminosity of the Fe  $K\alpha$  line in CT Sy2s is systematically lower than that of Sy1s and Sy2s for the same MIR luminosity. This implies that i) the Fe  $K\alpha$  luminosity cannot be used to estimate the intrinsic bolometric luminosity of AGN, ii) care should be taken when studying the luminosity function of CT Sy2s, iii) the X-ray spectral analysis of obscured type-II AGN should also take into account absorption of the reflection component. We estimated that on average, in Compton-thin and CT Sy2s, the reflected radiation is seen through a column density which is about 1/4 of the one absorbing the primary X-ray emission.

- We found the first significant evidence of X-ray Baldwin effect in Seyfert 2s. Our study has shown that for Sy2s  $L_{K\alpha}/L_{10-50}$  decreases with  $L_{10-50}$  with the same slope observed in Sy1s (right panel of Fig. 8). This implies that the mechanism responsible for this effect is the same in the two classes of AGN. If the mechanism responsible for the X-ray Baldwin effect is the  $\Gamma - \lambda_{\text{Edd}}$  correlation, then the X-ray corona and the accretion flow are connected in a similar way in Sy1s and Sy2s. On the other hand, if the X-ray Baldwin effect is due to luminosity-dependent unification of AGN, then our results show that the decrease of the covering factor of the torus in Sy2s is similar to that of Sy1s.

**Table A1.** 10–50 keV (1) and Fe  $K\alpha$  (2) luminosities for the LINERs and type-I AGN of the *Suzaku* sample of Fukazawa et al. (2011).

Source	(1) $\log L_{10-50}$	(2) $\log L_{K\alpha}$
<b>LINERs</b>		
M81	40.39	37.92
M106	41.17	38.67
<b>Type-I AGN</b>		
1H 0419–577	44.94	42.10
3C 120	44.23	41.80
3C 382	44.66	42.12
3C 390.3	44.67	42.12
4C +74.26	45.16	42.58
ARK 120	44.06	41.76
Fairall 9	44.29	42.14
IC 4329A	44.07	41.55
IGR J16185–5928	43.57	41.26
IGR J21247+5058	44.18	41.23
IRAS 18325–5926	43.40	40.95
MCG+8–11–11	44.06	41.75
MCG–6–30–15	42.96	40.42
Mrk 79	43.44	41.39
Mrk 110	43.97	41.48
Mrk 335	43.48	41.10
Mrk 359	42.73	40.62
Mrk 509	44.31	41.87
Mrk 766	42.85	40.43
Mrk 841	43.95	41.51
NGC 3227	42.41	40.12
NGC 3516	43.17	40.99
NGC 3783	43.36	41.20
NGC 4051	41.39	39.14
NGC 4151	42.58	40.53
NGC 4593	42.68	40.68
NGC 5548	43.47	41.14
NGC 7213	42.49	40.22
Swift J0501.9–3239	43.12	40.73
Swift J2009.0–6103	43.33	40.71

## APPENDIX A: SUZAKU DATA

In Table A1 the values of the 10–50 keV and Fe  $K\alpha$  luminosities for the LINERs and type-I AGN of the *Suzaku* sample of Fukazawa et al. (2011) are listed. Table A2 reports the same properties of Table A1 for the type-II and CT AGN, plus the absorption-corrected luminosities. The approach adopted to correct the luminosities is reported in Sect. 2.2.

## ACKNOWLEDGMENTS

We thank the referee for his/her comments, that significantly helped to improve the quality of the manuscript. We thank Chin Shin Chang for her comments on the manuscript. CR is a Fellow of the Japan Society for the Promotion of Science (JSPS). This work was partly supported by the Grant-in-Aid for Scientific Research 23540265 (YU) from the Ministry of Education, Culture, Sports, Science and Technology of Japan (MEXT). PG acknowledges support from STFC grant reference ST/J003697/1. This research has made use of the NASA/IPAC Extragalactic Database (NED) which

is operated by the Jet Propulsion Laboratory, of data obtained from the High Energy Astrophysics Science Archive Research Center (HEASARC), provided by NASA's Goddard Space Flight Center, and of the SIMBAD Astronomical Database which is operated by the Centre de Données astronomiques de Strasbourg.

**Table A2.** Observed (1) and absorption corrected (2) 10–50 keV luminosities, and Fe  $K\alpha$  luminosities (3) for the Type-II and CT AGN of the sample of Fukazawa et al. (2011).

Source	(1) $\log L_{10-50}^{\text{obs}}$	(2) $\log L_{10-50}$	(3) $\log L_{K\alpha}$
<b>Type-II AGN</b>			
3C 33	44.31	44.51	41.86
3C 105	44.51	44.66	42.18
3C 445	44.38	44.50	41.99
3C 452	44.48	44.68	42.05
Centaurus A	42.72	42.78	40.34
ESO 263-G013	43.67	43.76	41.14
MCG+04-48-002	43.21	43.46	40.59
MCG-5-23-16	43.51	43.63	41.17
Mrk 3	43.53	43.80	41.30
Mrk 417	43.89	44.06	41.28
Mrk 1210	43.18	43.31	40.80
NGC 1052	41.99	42.09	39.70
NGC 1365	42.51	42.55	39.95
NGC 2110	43.56	43.62	41.02
NGC 3281	43.25	43.48	40.87
NGC 4388	43.28	43.42	41.08
NGC 4395	40.51	40.52	37.95
NGC 4507	43.38	43.60	41.24
NGC 4992	43.66	43.84	41.30
NGC 5506	43.22	43.24	40.82
NGC 6300	42.38	42.46	39.91
NGC 7172	43.35	43.40	40.79
NGC 7314	41.93	41.94	39.83
NGC 7582	42.40	42.60	40.08
Swift J0138.6-4001	43.72	43.93	41.35
Swift J0318.7+6828	44.32	44.38	41.90
Swift J0505.7-2348	44.10	44.17	41.60
Swift J0601.9-8636	41.99	42.25	40.25
Swift J0959.5-2258	42.87	43.15	40.55
Swift J1200.8+0650	43.92	43.99	41.33
Swift J1628.1+5145	44.46	44.53	41.76
Mrk 1239	42.84	43.01	40.46
NGC 2273	41.92	42.22	40.26
NGC 1142	43.92	44.14	41.54
<b>CT AGN</b>			
Circinus Galaxy	41.65	42.01	39.88
ESO 323-G032	42.46	42.86	40.56
ESO 506-G027	43.58	43.90	41.48
IRAS 19254-7245	44.05	44.99	40.98
Mrk 1073	42.90	43.59	40.63
Mrk 273	43.46	43.87	41.04
NGC 1068	41.94	42.28	40.28
NGC 1386	41.28	41.90	39.06
NGC 3079	41.86	42.50	39.15
NGC 3393	42.68	43.02	40.22
NGC 4945	42.11	42.84	39.47
NGC 5135	42.74	43.39	40.57
NGC 5728	42.90	43.27	40.58

## REFERENCES

- Antonucci R., 1993, *ARA&A*, 31, 473
- Baumgartner W. H., Tueller J., Markwardt C., Skinner G., 2010, in *AAS/High Energy Astrophysics Division #11*, vol. 42 of *Bulletin of the American Astronomical Society*, 675
- Beckmann V., Soldi S., Ricci C., et al., 2009, *A&A*, 505, 417
- Bianchi S., Guainazzi M., Matt G., Fonseca Bonilla N., 2007, *A&A*, 467, L19
- Brusa M., Gilli R., Comastri A., 2005, *ApJ*, 621, L5
- Burlon D., Ajello M., Greiner J., Comastri A., Merloni A., Gehrels N., 2011, *ApJ*, 728, 58
- Chaudhary P., Brusa M., Hasinger G., Merloni A., Comastri A., Nandra K., 2012, *A&A*, 537, A6
- Comastri A., Iwasawa K., Gilli R., et al., 2010, *ApJ*, 717, 787
- Corral A., Della Ceca R., Caccianiga A., et al., 2011, *A&A*, 530, A42
- Corral A., Page M. J., Carrera F. J., et al., 2008, *A&A*, 492, 71
- Dadina M., 2008, *A&A*, 485, 417
- Dauser T., Wilms J., Reynolds C. S., Brenneman L. W., 2010, *MNRAS*, 409, 1534
- Diamond-Stanic A. M., Rieke G. H., Rigby J. R., 2009, *ApJ*, 698, 623
- Falocco S., Carrera F. J., Corral A., et al., 2013, *A&A*, 555, A79
- Fukazawa Y., Hiragi K., Mizuno M., et al., 2011, *ApJ*, 727, 19
- Gandhi P., Fabian A. C., Suebsuwong T., Malzac J., Miniutti G., Wilman R. J., 2007, *MNRAS*, 382, 1005
- Gandhi P., Horst H., Smette A., et al., 2009, *A&A*, 502, 457
- Giacconi R., Gursky H., Paolini F. R., Rossi B. B., 1962, *Physical Review Letters*, 9, 439
- Gilli R., Comastri A., Hasinger G., 2007, *A&A*, 463, 79
- Grandi P., Malaguti G., Fiacchi M., 2006, *ApJ*, 642, 113
- Grimes J. A., Rawlings S., Willott C. J., 2004, *MNRAS*, 349, 503
- Guainazzi M., Siemiginowska A., Stanghellini C., Grandi P., Piconcelli E., Azubike Ugwoke C., 2006, *A&A*, 446, 87
- Haardt F., Maraschi L., 1991, *ApJ*, 380, L51
- Ichikawa K., Ueda Y., Terashima Y., et al., 2012, *ApJ*, 754, 45
- Ikeda S., Awaki H., Terashima Y., 2009, *ApJ*, 692, 608
- Isobe T., Feigelson E. D., Nelson P. I., 1986, *ApJ*, 306, 490
- Iwasawa K., Mainieri V., Brusa M., et al., 2012, *A&A*, 537, A86
- Iwasawa K., Taniguchi Y., 1993, *ApJ*, 413, L15
- Jiang P., Wang J. X., Wang T. G., 2006, *ApJ*, 644, 725
- Jiménez-Bailón E., Piconcelli E., Guainazzi M., Schartel N., Rodríguez-Pascual P. M., Santos-Lleó M., 2005, *A&A*, 435, 449
- Jin C., Ward M., Done C., 2012, *MNRAS*, 425, 907
- Laor A., 1991, *ApJ*, 376, 90
- Lightman A. P., White T. R., 1988, *ApJ*, 335, 57
- Liu T., Wang J.-X., 2010, *ApJ*, 725, 2381
- Magdziarz P., Zdziarski A. A., 1995, *MNRAS*, 273, 837
- Maiolino R., Shemmer O., Imanishi M., et al., 2007, *A&A*, 468, 979
- Marshall F. E., Boldt E. A., Holt S. S., et al., 1980, *ApJ*, 235, 4
- Matt G., 2002, *MNRAS*, 337, 147
- Matt G., Fabian A. C., Ross R. R., 1996, *MNRAS*, 278, 1111
- Matt G., Guainazzi M., Frontera F., et al., 1997, *A&A*, 325, L13
- Matt G., Perola G. C., Piro L., 1991, *A&A*, 247, 25
- Miniutti G., Fabian A. C., 2004, *MNRAS*, 349, 1435
- Mitsuda K., Bautz M., Inoue H., et al., 2007, *PASJ*, 59, 1
- Morrison R., McCammon D., 1983, *ApJ*, 270, 119
- Murphy K. D., Yaqoob T., 2009, *MNRAS*, 397, 1549
- Nandra K., George I. M., Mushotzky R. F., Turner T. J., Yaqoob T., 1997, *ApJ*, 488, L91
- Nandra K., O'Neill P. M., George I. M., Reeves J. N., 2007, *MNRAS*, 382, 194
- Nayakshin S., 2000, *ApJ*, 534, 718
- Page K. L., O'Brien P. T., Reeves J. N., Turner M. J. L., 2004, *MNRAS*, 347, 316
- Patrick A. R., Reeves J. N., Porquet D., Markowitz A. G., Braitov V., Lobban A. P., 2012, *MNRAS*, 426, 2522
- Ponti G., Cappi M., Costantini E., et al., 2013, *A&A*, 549, A72
- Ricci C., Paltani S., Awaki H., Petrucci P.-O., Ueda Y., Brightman M., 2013a, *A&A*, 553, A29
- Ricci C., Paltani S., Ueda Y., Awaki H., 2013b, *MNRAS*, 435, 1840
- Ricci C., Ueda Y., Ichikawa K., et al., 2014, *ArXiv e-prints*
- Ricci C., Walter R., Courvoisier T. J.-L., Paltani S., 2011, *A&A*, 532, A102
- Risaliti G., Young M., Elvis M., 2009, *ApJ*, 700, L6
- Schmitt J. H. M. M., 1985, *ApJ*, 293, 178
- Shemmer O., Brandt W. N., Netzer H., Maiolino R., Kaspi S., 2008, *ApJ*, 682, 81
- Shu X. W., Wang J. X., Yaqoob T., Jiang P., Zhou Y. Y., 2012, *ApJ*, 744, L21
- Shu X. W., Yaqoob T., Wang J. X., 2010, *ApJS*, 187, 581
- Shu X. W., Yaqoob T., Wang J. X., 2011, *ApJ*, 738, 147
- Simpson C., 2005, *MNRAS*, 360, 565
- Treister E., Urry C. M., Virani S., 2009, *ApJ*, 696, 110
- Türler M., Chernyakova M., Courvoisier T. J.-L., et al., 2010, *A&A*, 512, A49
- Turner T. J., Pounds K. A., 1989, *MNRAS*, 240, 833
- Ueda Y., Akiyama M., Ohta K., Miyaji T., 2003, *ApJ*, 598, 886
- Vasudevan R. V., Mushotzky R. F., Gandhi P., 2013, *ApJ*, 770, L37
- Wilms J., Allen A., McCray R., 2000, *ApJ*, 542, 914
- Wright E. L., Eisenhardt P. R. M., Mainzer A. K., et al., 2010, *AJ*, 140, 1868
- Yaqoob T., Murphy K. D., 2011, *MNRAS*, 412, 277
- Yaqoob T., Padmanabhan U., 2004, *ApJ*, 604, 63
- Zhou X.-L., Wang J.-M., 2005, *ApJ*, 618, L83